Published in final edited form as:
J Nucl Cardiol. 2020 December ; 27(6): 2083–2099. doi:10.1007/s12350-019-01973-9.

Hybrid PET/MR imaging in myocardial inflammation post-myocardial infarction

B. Wilk, BSc[a,b,c], **G. Wisenberg, MD**[a,d], **R. Dharmakumar, PhD**[e,f], **J. D. Thiessen, PhD**[a,b,c], **D. E. Goldhawk, PhD**[a,b,c], **F. S. Prato, PhD**[a,b,c]

[a]Department of Medical Imaging, Western University, London, Canada

[b]Lawson Health Research Institute, London, Canada

[c]Collaborative Graduate Program in Molecular Imaging, Western University, London, Canada

[d]MyHealth Centre, Arva, Canada

[e]Biomedical Research Institute, Cedars-Sinai Medical Center, Los Angeles, CA

[f]David Geffen School of Medicine, University of California, Los Angeles, CA

Abstract

Hybrid PET/MR imaging is an emerging imaging modality combining positron emission tomography (PET) and magnetic resonance imaging (MRI) in the same system. Since the introduction of clinical PET/MRI in 2011, it has had some impact (e.g., imaging the components of inflammation in myocardial infarction), but its role could be much greater. Many opportunities remain unexplored and will be highlighted in this review. The inflammatory process post-myocardial infarction has many facets at a cellular level which may affect the outcome of the patient, specifically the effects on adverse left ventricular remodeling, and ultimately prognosis. The goal of inflammation imaging is to track the process non-invasively and quantitatively to determine the best therapeutic options for intervention and to monitor those therapies. While PET and MRI, acquired separately, can image aspects of inflammation, hybrid PET/MRI has the potential to advance imaging of myocardial inflammation. This review contains a description of hybrid PET/MRI, its application to inflammation imaging in myocardial infarction and the challenges, constraints, and opportunities in designing data collection protocols. Finally, this review explores opportunities in PET/MRI: improved registration, partial volume correction, machine learning, new approaches in the development of PET and MRI pulse sequences, and the use of novel injection strategies. (J Nucl Cardiol 2019)

Reprint requests: B. Wilk, BSc, Department of Medical Imaging, Western University, London, Canada; bwilk@uwo.ca.

Electronic supplementary material The online version of this article (https://doi.org/10.1007/s12350-019-01973-9) contains supplementary material, which is available to authorized users.

The authors of this article have provided a PowerPoint file, available for download at SpringerLink, which summarizes the contents of the paper and is free for re-use at meetings and presentations. Search for the article DOI on SpringerLink.com.

The authors have also provided an audio summary of the article,which is available to download as ESM, or to listen to via theJNC/ASNC Podcast.

Disclosures
All authors have no potential conflicts of interest.

Keywords

Myocardial biology; inflammation; myocardial ischemia and infarction; MRI; PET; hybrid imaging

INTRODUCTION

Although early mortality in patients with acute myocardial infarction (AMI) has declined by 75% over the past half century[1], these patients still remain at risk for late adverse events and death[2]. Evidence suggests that infarct size[3,4], extent of microvascular obstruction within infarcted tissue,[5] and extent of iron precipitation[6–8] following hemorrhagic infarction are independent predictors of left ventricular remodeling post-AMI, leading to heart failure. Furthermore, this remodeling is associated with additional effects on myocardial tissue remote from the AMI caused by an ongoing dysregulated pro-inflammatory process[9,10]. The target/substrate to be imaged in post-myocardial infarction is predominantly inflammatory cells responding to aseptic injury. There is also growing evidence that the presence of iron in the infarcted tissue following a hemorrhagic infarct plays a further role in modulation of inflammation[6,8].

Role of Inflammatory Cells

After AMI, pro-inflammatory processes stabilize the region of infarction with scar tissue that strengthens the muscle to prevent the development of an aneurysm and reduce the potential for sudden death from cardiac rupture[11–13]. Two cellular hallmarks of this pro-inflammatory stage include neutrophils[14] (peaking within the first few hours to days post-MI in humans and dogs) and classically activated (M1) macrophages (peaking between 3 and 10 days post-MI in humans and dogs)[6,15–20]. The population of M1 macrophages is primarily of myeloid origin, but may also include tissue resident macrophages within the myocardium and those drawn from splenic reservoirs[21–24]. These are the dominant inflammatory cell types responding to MI. The pro-inflammatory period is followed by an anti-inflammatory stage where the predominant cellular hallmark is the recruitment of alternatively activated (M2) macrophages[13]. Note that M1 and M2 macrophages are a simplification and the picture is more complex with in-between macrophage phenotypes and the possibility for the polarization to change[25,26]. Although it has been suspected that progression to heart failure post-AMI is related to a sustained pro-inflammatory response[27,28], anti-inflammatory clinical trials have yielded mixed results[29]. If anti-inflammatory therapies are given too early to reduce the “healing” inflammatory response, the patients are at increased risk of aneurysm; if administered too late, there is an increased risk of negative local and remote myocardial tissue remodeling. In order to develop effective therapies tailored to modify this dynamic process towards improved clinical outcomes, a non-invasive cardiac imaging method is required to detect the differential time course, post-AMI, of the inflammatory processes in three myocardial tissues: (a) infarcted tissue with microvascular obstruction (i.e., infarcted obstructed tissue, IOT), (b) infarcted tissue excluding the zone of microvascular obstruction (i.e., infarcted not obstructed tissue, INOT), and (c) myocardial tissue remote from the infarcted tissue (i.e., remote tissue, RT). These tissues may have vastly different patterns and timing of the inflammatory response. However, if the appropriate therapy could be tailored for each patient early in the management and progression of the disease process, using non-invasive imaging to differentiate between neutrophils, M1 and M2 macrophages, then we could optimize therapy in real time, inform treatment, and personalize care.

Given their divergent effects, non-invasive imaging that distinguishes between M1 and M2 macrophages is critical and hence an understanding of the differences that could be exploited for imaging is essential. Glucose uptake in M1 macrophages is approximately twice that of M2 macrophages and phagocytic activity of M2 is approximately twice that of M1[30,31]. Also, macrophage phenotype may be distinguished based on iron handling, as M1 exhibit an iron storage phenotype while M2 display an iron recycling phenotype[32,33]. Macrophages are among the few mammalian cells to express the only recognized mammalian iron export protein, ferroportin. Its activity is subject to regulation by the endocrine hormone hepcidin, produced primarily in the liver in response to pro-inflammatory cytokines, like inter-leukin-6, and elevated levels of iron. Systemic hepcidin-ferroportin interactions induce ferroportin degradation and interrupt iron export[34]. In the dog, serum hepcidin levels rise within 4–6 days post-MI (unpublished data), facilitating the production of M1 macrophages and locally depriving the injured tissue of iron. In the canine model of myocardial hemorrhage, Kali et al[6] suggest that elevated iron stalls macrophage progression from M1 to M2, consistent with the interaction of hepcidin and ferroportin. This in turn may delay the evolution of M2 activities needed to stabilize the scar, like fibroblast formation, and may also damage RT by prolonging the pro-inflammatory activity of M1 macrophages.

MRI OF MYOCARDIAL INFLAMMATION

Post-MI MRI is an attractive modality to use due to its high spatial resolution, excellent soft tissue contrast, and ability to mitigate and/or measure cardiac and respiratory motion.

Functional Imaging

The capability of MRI to acquire “cine” images of wall motion throughout the cardiac cycle during breath holds has resulted in cardiac MRI becoming effectively the gold standard for the quantitation of ejection fraction, end-diastolic volumes, and end-systolic volumes, all important in the definition of cardiac function with respect to progression towards heart failure. The imaging of left ventricle wall strain showing wall fiber tracks has not been as important. Although developed in the 1990s,[35] it has yet to establish itself for discriminating INOT and IOT[36]. The imaging of smaller cardiac structures such as those associated with the atria has been more difficult due to the thinness of the atrial wall, approaching the resolution of MRI. Developments such as phase contrast flow imaging, where the velocity of moving magnetic moments (flow) is proportional to the phase shift[37], and its successor, 4D Flow, have been helpful in estimating effects of valve defects on regurgitant fraction in the ventricles[38]. Attempts to apply 4D Flow to investigate effects of atrial fibrillation are in development[39].

“Scar” Imaging

It has been shown extensively that the distribution volume of gadolinium chelates such as Gd-DTPA corresponds to the extracellular space in the myocardium. This is calculated as the ratio of the concentration of Gd-chelate in the myocardium divided by the concentration in the blood, which is often referred to as the partition coefficient and designated as λ. The volume of distribution can be calculated from λ if the hematocrit is known, i.e., $V_d = \lambda \times (1 - \text{Hct})$. It has been shown in both humans and dogs that λ in myocardial tissue post-MI increases from approximately 0.45 to 0.9 mL g^{-1}[40–42]. For a hematocrit of 0.4, this would correspond to volumes of distribution going from 0.27 to 0.54 mL g^{-1}. It has also been shown that (a) this increase occurs within a few hours of occlusion/reperfusion injury[42], (b) that it may be reduced when the post-MI injury has become chronic[42,43], (c) it represents a marker of permanently damaged myocardium[44], as reversible injury such as stunning[40] or hibernation[45] does not increase λ substantially,[46] and (d) given MRI’s spatial resolution, it allows the transmural extent of the infarct to be determined[47,48]. Non-contrast-enhanced scar imaging approaches have also demonstrated that scar following MI can be characterized on the basis of T1 mapping using modified look-locker with balanced steady-state free-precession readouts at 3.0 T[49,50].

Edema Imaging

The T2 relaxation rate increases in tissue containing an increase in extracellular water, i.e., edema, resulting in a hyperintense signal in T2-weighted MRI. The extent to which edema correlates with the extent of inflammation post-MI still needs to be determined.

Iron Detection

T2*-weighted cardiac MR is effective in the detection and characterization of infarction/reperfusion-induced myocardial hemorrhage[7,8,51]. Histological study of canine myocardial infarction has shown that persistent microvascular obstruction post-MI culminates in the development of ferric iron oxide crystals, an increased pro-inflammatory burden and adverse remodeling. A postulated mechanism is that the conversion from M1 to M2 macrophages may be delayed by this iron crystal formation leading to dysregulation of the inflammatory response and progression to heart failure and/or an aneurysm at the site of infarction[6]. However, in vivo validation of this hypothesis requires the non-invasive differential imaging of M1 and M2 macrophages at the site of iron accumulation.

Myocardial Blood Flow

Myocardial blood flow is a major consideration when discussing myocardial inflammation as it may play a major role in the degree and extent of the process. Myocardial blood flow can be measured following a bolus injection of a gadolinium chelate with transmural resolution[52,53]. However, complete heart coverage may not always be possible and two bolus injections to account for signal saturation are often employed[54,55], increasing the amount of Gd-chelate that is needed though methods are being developed to overcome these issues. Comparison to determinations using PET has indicated the increased complexity of the use of Gdchelates which have a much lower extraction fraction compared to PET methods such as those using ^{13}N-Ammonia or ^{15}O-water[56–58]. It is important to note here that ^{13}N-Ammonia enters and is trapped in living cells while Gd-chelates are extracellular[59].

BOLD MRI Contrast

Blood Oxygen Level-Dependent (BOLD) contrast in MRI has been extensively applied for the noninvasive study of the brain. Due to the decreased extraction fraction of oxygen when blood flow increases, venous blood contains higher levels of oxyhemoglobin with a corresponding decrease in the concentration of deoxyhemoglobin. When the venous deoxyhemoglobin concentration falls, then T2* increases. Hence, the BOLD effect is an indication of the venous concentration of deoxyhemoglobin. Li et al[60] have shown in normal volunteers that following the administration of the hyperemic agent, dipyridamole, with increased myocardial blood flow, there is an increase in T2* which is consistent with a decrease in myocardial venous deoxyhemoglobin concentration as myocardial oxygen supply exceeds demand[60]. In contrast, the administration of dobutamine resulted in an increase in coronary blood flow but no significant change in T2* consistent with a lack of change in myocardial venous deoxyhemoglobin concentration which is interpreted as a balance between oxygen supply and demand. This seminal work laid the foundation for future applications. However, not until recently has the BOLD measurement in the myocardium been of sufficient accuracy to be used in routine cardiac assessment. Recently, new MRI methods for the measurement of cardiac BOLD have shown considerable promise indicating a potential to assess myocardial ischemia comparable with SPECT and PET methodologies[61]. As this has now been demonstrated in a canine model of ischemia, clinical studies demonstrating feasibility are needed.

Chemical Exchange Saturation Transfer (CEST)

Chemical exchange saturation transfer (CEST) relies on the selective saturation and exchange of protons from metabolites of interest to the free protons imaged with MRI[62–64]. CEST has been used to detect changes in protein concentration[65], glutamate[66], creatine[67], glycosaminoglycan, and most notably pH (acidoCEST)[68,69] and D-glucose (glucoCEST)[70–72] though it can be difficult to unravel changes in CEST signal from changes in pH, T1, temperature, and other metabolites[73]. To our knowledge, neither glucoCEST nor acidoCEST has been attempted in the heart, although there would be some utility for alternative measurements of perfusion and pH post-MI. Cardiac CEST acquisitions are challenging; however, recent promising results suggest its utility for measuring myocardial creatine kinase[74–76] and hyaluronan synthesis[77] post-MI.

Labeling Inflammatory Cells

Iron particles of magnetite are strong negative contrast agents attenuating the MRI signal through the strong susceptibility induced by ferromagnetism. Using iron particles to label cells has been investigated using two different approaches. In one, inflammatory cells are isolated from blood lymphocytes, labeled with iron particles (such as superparamagnetic iron oxide (SPIO) particles) and then re-injected[78]. In this scenario, detection of loss of MRI signal within the myocardium signifies the presence of labeled cells once the blood background is reduced, and provided the iron particles have not been released by dying lymphocytes and either engulfed by other cells or lodged in the extracellular space. This signal may also be confounded by endogenous iron due to hemorrhage. Although it has been shown that, under optimal conditions, individual cells can be seen, quantitation of label has proven challenging due to (a) the difficulty in relating the magnitude of the loss of MRI signal with the amount of iron particles[79] and (b) the dilution of the label as labeled cells proliferate. This effectively limits the quantitation of the number of cells. Note that labeling cells with positive contrast (e.g., ^{19}F) may overcome this issue but dilutions due to proliferation cannot be overcome[80–82]. In addition to phagocytic activity, monocytes and macrophages possess iron export activity that is detectable by MRI. In the human THP-1 monocyte cell line, iron export prevails regardless of extracellular iron concentration[83]. These cells display both autocrine/paracrine regulation of ferroportin as well as the endocrine response to hepcidin. In the multi-potent P19 cell line, extracellular iron stimulates iron export through transcriptional regulation, whereas the presence of hepcidin knocks it back down via post-translational modification[36,84–86]. Thus, processes governing the up and downregulation of iron export co-exist and contribute an MR visible signal that will be influenced by proinflammatory signaling through hepcidin, the inherent iron recycling activity of M2 macrophages, and the iron released from SPIO degradation.

In the second approach, SPIO particles or perfluorocarbon agents are injected intravenously, hypothesizing that macrophages will engulf them and allow their detection. It has been shown in vitro that their engulfment rate in M2 macrophages is approximately 50% greater than for M1 macrophages[30]. However, using this method, the MRI signal will be related to the uptake of particles by both M1 and M2 macrophages, making it difficult to determine the relative contribution of each cell population to the signal change.

MRI reporter genes that deliver strong contrast have been difficult to develop[85]. One of the best approaches involves introducing genes from magnetotactic bacteria in mammalian cells for the biosynthesis of membrane-enclosed SPIO-like particles called magnetosomes[86]. The technology was initially attempted using single gene expression systems[87]. If this technology could be implemented such that the concentration of iron particles in mammalian cells was equal to that in magnetotactic bacteria, theoretical calculations indicate that as few as 3 cells could be detected in small animals and as few as 2,600 cells in large animals and humans[87]. This would correspond to a major breakthrough. For example, white blood cells from the peripheral circulation (e.g., monocytes) could be isolated and transfected with the MR reporter gene expression system, which could be programmed to produce magnetosome-like iron particles upon promoter activation. For example, the receptor gene could be engineered to signal, by production of iron particles, a molecular event involved in differentiation of the monocyte into an M1 macrophage. One of the main obstacles remaining is the acceptance of genetically modified cells for human use, although this strategy is now permitted in some therapeutic applications[88].

PET IMAGING POST-MYOCARDIAL INFARCTION

Although there are a large number of PET probes for cardiac investigation that have been developed, see Figure 1, clinical practice to date for use in post-MI patients has used only a few[89]. PET imaging post-MI is most commonly done with ^{18}F-FDG although suppression of healthy myocyte glucose uptake is needed concurrent with flow tracers to evaluate ischemia.

However, other tracers that target translocator protein (TSPO) receptors in inflammatory cells, such as ^{18}F-GE180 or ^{18}F-FEPPA, may be used to target macrophages specifically.

Glucose Metabolism

Inflammation can be measured with ^{18}F-FDG due to the increased presence of GLUT1 transporters on macrophages. Due to this, uptake of glucose is upregulated in areas of inflammation. The non-specificity of ^{18}F-FDG for evaluating cardiac inflammation is, however, compounded by uptake in normal myocytes which must be suppressed for successful, unambiguous detection of inflammation. The failure, at times, to effectively suppress that uptake by either dietary modification (high fat), overnight fasting, or heparin injection may result in failure of the test. Five percent of the time this test fails even under the best diet and fasting protocols[90]. The reduced spatial resolution of ^{18}F-FDG-PET compared to 3T MRI makes it difficult to uniquely identify ^{18}F-FDG uptake in the three tissue regions post-MI: IOT, INOT, and RT. Although in vivo cardiac imaging reflects the significant uptake by inflammatory cells, it may not allow the distinction between M1 and M2 inflammatory cells.

It has been shown in vitro that ^{18}F-FDG uptake in M1 macrophages is greater than in M2 macrophages. Uptake in M1 macrophage is twice that of M2 when differentiated from the human THP-1 monocyte cell line[30]. In contrast, when using primary monocytes from human blood, the uptake of ^{18}F-FDG in M1 macrophages is ten times greater than M2[91]. This is further obscured as uptake of ^{18}F-FDG by neutrophils and monocytes may be similar to that of M1 macrophages. Although compartmental analysis allows the quantitation of glucose metabolism in units of mmol per gram per minute, there has been little or no attempt to evaluate quantitative ^{18}F-FDG uptake post-MI in macrophages. The upregulation of ^{18}F-FDG metabolism in inflammatory cells must be very large for this to be seen in infarcted tissue since the density of inflammatory cells in infarcted tissue would be much lower than that of myocytes in normal and remote tissue. It is unknown at this time if myocardial suppression of ^{18}F-FDG uptake affects uptake of ^{18}F-FDG in inflammatory cells. However, work reported of ^{18}F-FDG studies in cardiac sarcoidosis indicates that if uptake is suppressed in inflammatory cells it is not sufficient to eliminate the strong signal of inflammation[92].

Blood Flow

Historically, PET myocardial blood flow measurements have used ^{13}N-Ammonia, ^{15}O water, or ^{82}Rb. At centers using PET/CT, ^{82}Rb is often used since it does not require an on-site cyclotron, as opposed to ^{13}N-Ammonia (10-minute half-life) and ^{15}O-water (2-minute half-life). However, the 82Rb positron range reduces effective spatial resolution and, to date, no manufacturer of ^{82}Rb/^{82}Sr generators has produced an MR-compatible system. In this context, ^{13}N-Ammonia is attractive for cyclotron-equipped sites and it has both high first pass extraction fraction and good retention characteristics[93]. However, the 10-minute half-life makes stress/rest studies expensive. More development of a repeat injection strategy would lower costs substantially by greatly reducing the length of the exam[94]. Alternatively, ^{18}F-flurpiridaz is attractive due to its very high extraction and retention characteristics, but the cost of the tracer may negatively impact its implementation. Additionally, the long half-life makes it difficult to conduct stress/rest exams during a single imaging session as the traditional approach requires waiting for the tracer to have decayed between the stress and the rest scans. Whereas the measurement of blood flow reserve is important in the scenario of stable coronary disease, its value post-MI has not been established. Perhaps its impact would be better known if PET blood flow studies, using ^{13}N-Ammonia, could be combined with inflammation using ^{18}F-FDG in the same imaging study. Perhaps, in the future this will be possible if repeat injection studies are developed and clinically implemented.

Imaging Macrophages

Many PET ligands have been developed to detect upregulation of the mitochondrial translocator protein (TSPO) in activated microglia, the tissue resident macrophages of the brain[95]. However, it is not known to what extent TSPO upregulation distinguishes between pro- and anti-inflammatory macrophages. In addition, there is the added limitation that a polymorphism affects TSPO binding[96]. Recently, it has been shown[97] in mice and humans that myocardial inflammation post-MI could be detected using a TSPO-PET ligand. However, in vitro work[91] suggests that this compound is taken up by other inflammatory cells besides M1 macrophages. (It has been reported that the uptake in M1 macrophages is four times greater than the uptake in M2 macrophages, neutrophils, monocytes, T/MK cells, and B cells.[91]) The one real advantage over ^{18}F-FDG is that uptake of TSPO-PET ligands in the normal myocardium does not have to be suppressed in order to detect inflammatory cells remote from the infarcted tissue. However, almost all research has been related to uptake in microglia and there is a need for more research into the in vivo uptake of TSPO-PET ligands by inflammatory cells.

Injecting Labeled Inflammatory Cells

Although labeling white blood cells has been practiced in nuclear medicine for decades to detect sites of inflammation, imaging these cells within the myocardium has not been possible[98]. This is due to (a) partial volume effects and (b) the lack of retention of the tracer within the labeled cells[99]. As it has been demonstrated that ^{111}In-labeled white blood cells do accumulate in the IOT if injected approximately 24 hours prior to sacrifice, further imaging innovation to achieve the goal of imaging labeled inflammatory cells in the IOT may be worthwhile[100]. A recently developed new PET probe (^{89}Zr-DBN) that labels the (white blood) cell plasma membrane in a stable manner[99] addresses tracer leakage. The attractiveness of a ^{89}Zr label is its long half-life (3.3d) which would allow the initial high background activity in the left ventricular cavity to be reduced/cleared, though this also leads to a potential for somewhat higher radiation exposure from this isotope, similar to what is seen in ^{111}In-labeled white blood cells[99]. However, effective implementation will require high spatial resolution anatomic images of the heart (by CT or MRI) that are reliably registered to the PET image to allow for effective partial volume correction and confidence in the location of regions of interest corresponding to IOT, INOT, and RT identification. Although quantitation of the ^{89}Zr signal is relatively simple and reliable compared to quantitation of SPIO iron particles by MRI, there is still the problem of quantitation of the number of cells. Obtaining the absolute number of cells rather than a relative amount of inflammation would be ideal for determining the efficacy of anti-inflammatory therapy, comparison to histology, or future research into the mechanism of inflammation post-MI.

Inflammatory cell proliferation and resultant dilution of the label interferes with reliable quantitation. As has been shown by Blackwood et al, one likely advantage over MRI is that, as cells die, ^{89}Zr-labeled debris will likely not be engulfed by other cells[101], whereas the SPIO particles released by labeled cells as they die have been reported trapped in other cells and in the interstitium of the myocardium[102,103]. Reporter genes have also been developed for PET. Cells that are transfected and transplanted directly into the myocardium can be visualized after injection of the needed radiolabeled substrate[104,105]. To date, tracking intravenously injected PET reporter gene-expressing cells within IOT, INOT, and RT has not been accomplished and there remains the general prohibition of injecting genetically modified cells into humans. Nevertheless, it might be worth investigating if ^{89}Zr-labeled cells could be developed that would allow visualization of inflammatory cells in the IOT, INOT, and RT regions, if hybrid PET/MRI were used to identify the anatomical location of the ^{89}Zr activity. Figure 1 summarizes the currently available PET probes and MRI agents discussed.

HYBRID PET/MR TECHNOLOGY

In Figure 2, the sensitivity, spatial resolution, and approximate maximum sample diameter of PET and MRI are compared and contrasted with other major imaging modalities (SPECT, CT, and optical) for large animal and human imaging. It should be emphasized that hybrid PET/MRI is a convergence of PET and MRI and unlike PET/CT, which is a sequential acquisition technology, hybrid PET/MRI allows simultaneous acquisition over the same anatomical site. As such, although both PET and MRI are mature technologies when used independently, their combination with hybrid PET/MRI adds a distinct additional nuance that may take many years to explore and determine the value of hybrid PET/MRI over sequential PET and MRI.

The engineering feat of integrating a PET ring into the bore of an MRI required a major redesign of whole-body PET technology[106]. The equipment challenges that remain include (a) optimization of the RF/MRI receive coils to reduce the attenuation of the PET signal while maintaining similar performance to dedicated MRI only coils and (b) MR-based PET attenuation correction (MRAC) that compares well with CT-based PET attenuation correction (CTAC). A recent publication demonstrated high MR performance and low PET signal attenuation with a 32-channel RF array designed prospectively for cardiac PET/MRI[107]. Furthermore, MR-derived attenuation correction of the heart using manufacturer-provided software shows excellent correlation with corrections using CT[106,108,109].

Hybrid PET/MR in Cardiology

The major limitation in standalone PET (i.e., sequential PET/CT) has been the collection of data while the heart moves through the combined cardiac and respiratory cycles. This is in contrast to cardiac MRI, wherein ECG synchronization of the cardiac cycle can be combined with breath hold or respiratory gating[110]. However, respiratory gating of PET results in loss of 50% of the data and dividing the cardiac cycle into eight phases results in a total loss of 15/16th of the collected data for each component phase. Methods have been developed to register cardiac MR images taken at different times in the respiratory cycle[111,112] but to date they have not been effectively used to reduce/eliminate the effect of motion on the PET data without sacrificing some MRI capabilities[113–116]. It is possible that the respiratory and cardiac motion of the heart could be tracked by MRI (e.g., with 3D navigator echoes and motion-sensitive MRI acquisitions) and PET lines of response shifted to a fixed cardiac location (e.g., end diastole at functional residual capacity)[117].

Accurate registration to MRI is needed to effectively implement partial volume correction of cardiac PET. Although conceptually simultaneous PET/MRI over the heart has the needed information, this has yet to be achieved. Figure 3 shows the importance of PET registration to MR to relate the extent of inflammation to the post-MI tissue types defined by contrast-enhanced MRI. Also, with good suppression of normal ^{18}F-FDG myocyte uptake, it is only by MRI registration that the extent of ^{18}F-FDG uptake associated with the different post-MI tissue types can be identified. The appeal of “perfect” registration is shown in Figure 4 where the FDG-PET and post-contrast MRI images are perfectly registered as the data were taken after euthanasia[100]. Notice the potential for subtransmural PET signal localization.

Future Opportunities with Hybrid Cardiac PET/MRI

Prior to hybrid imaging in PET (i.e., PET/CT), the use of PET radiopharmaceuticals was dependent on low (but not zero) non-specific binding for anatomical localization of signal. With automatic registration of the MRI image to the PET distribution, the trend to develop PET probes without non-specific binding can now be further engaged without the need of additional radiation dose from CT. For example, this enables the tracking of PET labeled cells. As outlined in the section “Injecting Labeled Inflammatory Cells,” the tracking of ^{89}Zr-labeled cells would be possible if hybrid PET/MRI reliably registered the PET and MRI images, whereas this may not be reliably done with PET/CT or sequential PET/MR. ^{89}Zr with its 3.3-day half-life is attractive for longitudinal imaging since it can be tracked within the body for as long as 30 days[118].

Hybrid PET/MRI Protocols

An opportunity and challenge for hybrid PET/MRI is to optimize the combined PET and MRI protocols. One of the issues post-MI is delivery to an area of IOT. A bolus injection of gadolinium chelate does not penetrate IOT and hence allows its discrimination from the INOT. Although this lack of penetration of the MR contrast agent allows the discrimination of the three post-MI tissue types, the lack of penetration of ^{18}F-FDG blocks information regarding the presence or absence of inflammatory cells in the IOT. A bolus injection of ^{18}F-FDG does not penetrate this zone sufficiently to give inflammatory cells the opportunity to sequester the tracer[100]. A novel and now possible approach would be to maintain a high blood concentration of tracer for a sufficiently long period of time to allow increased delivery of the tracer, even to the regions of severely compromised flow. This could be accomplished by a constant infusion of ^{18}F-FDG and a Gd-chelate. If the Gd-chelate were able to penetrate the IOT during a 40-minute infusion, then it is likely that ^{18}F-FDG would also be delivered sufficiently to somewhat penetrate IOT and INOT. A slow infusion would allow accurate 3D T1 maps to be collected as tissue concentrations would not change appreciably during the acquisition and this would match the 3D data collection of ^{18}F-FDG-PET. Normally 3D T1 maps cannot be accurately collected after a bolus injection of Gd-chelate. This would provide unprecedented 3D data matched in time and space between ^{18}F-FDG-PET and Gd-chelate/MRI. As the concentration of Gd-chelate would not change appreciably during the 3D T1 map data collection, subtle changes in the extracellular volume could be detected in the remote myocardium[119–121].

One of the major differences between PET and MRI is the flexibility in binning the data after the acquisition. PET data can be collected in list-mode, where the location and time of individual PET events is recorded in a large raw data file. If physiological timing markers are also recorded, it is possible to reconstruct PET images at any point within the respiratory and cardiac phases, hence allowing the elimination of data corrupted by motion of either physiological origin and/or associated with patient bulk movement. MRI data are typically collected in a rigid format corresponding to a patterned projection in k-space and MRI images are difficult to accurately reconstruct from an incomplete set of k-space data. Recently, this constraint of MRI has been addressed using a novel approach to randomize k-space data collection that would then allow matching in time of MRI with "random" PET list-mode image creation[122–125]. This will harmonize the way PET and MRI data is collected and used, which is important to fully realize the benefits of simultaneous acquisition such as improved PET to MRI registration.

Hybrid PET/MRI as a Convergent Technology

The convergence of PET and MRI will provide medical imaging with a new imaging modality. To achieve convergence, there is a need for near-perfect registration between PET and MRI as well as other factors outlined in Figure 5. A major limitation of PET is the one common signal (511 keV annihilation radiation) for all PET radioisotopes. This limits PET to a single radiopharmaceutical during any one data collection, whereas in MRI there is the capacity to collect a variety of image contrasts based on different pulse sequences and interactions of protons with static and varying magnetic fields. For example, a post-MI study that requires both blood flow (e.g., ^{13}N ammonia) and inflammation (e.g., ^{18}F-FDG) by PET is difficult to achieve in a single imaging session. One possibility is to perform myocardial blood flow measurements using contrast-enhanced MRI[126] or BOLD MRI[127] which could reduce acquisition time and dose during cardiac examinations, as shown in Figure 6. This would be especially useful in diseases such as cardiac sarcoidosis where it would be advantageous to study blood flow and inflammation[92,128]. Reducing the acquisition time and dose would allow investigators to try new studies which would presently not be possible due to the length of the scan and the patient's ability to withstand it. One potential with hybrid PET/MRI is the use of the Tofts model[129] to quantify K_{trans}, a transfer constant related to tissue perfusion, during a constant infusion and how this relates to PET tracer dynamics[130]. The replacement of FDG-PET with glucoCEST is intriguing but issues with sensitivity of CEST and the fact that different glucose pools are being detected requires significant development[131]. CEST measurements sensitive to creatine kinase, hyaluronan synthesis, or pH may hold more promise in combination with complementary PET imaging.

Artificial Intelligence in Hybrid PET/MR

In an extensive state-of-the-art review on artificial intelligence in cardiovascular disease, cardiac PET and cardiac MRI are treated separately[132]. The major limitation for the application of AI to hybrid PET/MRI for the detection of disease is the absence of a large cohort of “ground truth” data needed for the training sets. Some of the outcomes of AI as applied separately to PET and MRI suggest some applications to improve the quality of information. For example, the 2016 Kuggle Data Science Bowl competition provides more than 1000 cardiac cine MR data sets and the AI developed has shown that left ventricular end-systolic and enddiastolic volumes can be determined[133]. If this approach could be used to identify these volumes and also the epicardial and the endocardial borders at the same respiratory and cardiac phases as in the PET data simultaneously collected, then this could allow identification of the location of these cardiac structures in the PET images, even if in the PET images these structures were not visible. Not only would this automation reduce image analysis, but it would also allow the identification of the same structures in the PET data. Unfortunately, to the best of our knowledge, the needed PET ground truth data are not available, even for the development of machine learning approaches to assist in the determination of diagnostic values. It would be of considerable value if there were cardiac PET/CT and MRI data of the same patients even if acquired separately. For example, the Alzheimer’s Disease Neuroimaging Initiative archived data sets include brain PET and MRI images of the same patient and would allow sufficient training sets to develop AI for joint PET/MRI reconstructions, partial volume correction, MR-derived attenuation correction, and dose reduction, to name a few. These findings, in turn, could be tested with true hybrid PET/MRI data sets. Unfortunately, there are no such large data sets for separate cardiac PET and cardiac MRI on the same patients. It seems inevitable that the data would have to be collected on hybrid PET/MRI systems to test joint reconstruction, kinetic modeling, and partial volume correction. As we have suggested already, optimizing AI outcomes of combined simultaneously acquired PET and MRI data will require data collection protocols which are very different than what is collected for standalone MRI. Both supervised and unsupervised approaches should be explored with respect to combined connected model analysis. The number of fitted parameters should be small and restricted in supervised approaches, whereas in the unsupervised approach many more parameters can be investigated[132]. Another example would be the use of MRI-guided PET reconstruction to reduce radiation dose by constraining the PET reconstruction to reduce the effect of noise.

A common AI approach is to try to simulate another, gold-standard modality, e.g., generating a pseudo-CT with MRI for MRAC or predicting Gd-enhanced images with non-contrast MRI. Can we use this approach with matched MRI and PET to predict regions of inflammation? That is, can we get enough information from multiparametric MRI (Gd-enhanced, blood flow, T2-weighted, T2*-weighted, and CEST) to predict where inflammation should be and validated with FDG-PET or TSPO-PET?

PRECLINICAL BENCH MARKING USING ANIMAL MODELS

Significant advances in cardiac imaging have often required the use of animal models allowing for the establishment of ground truth directly from tissue. Both small animal and large animal models have been effective. For example, most recently, Thackeray et al[97] used an infarct mouse model to test the use of a TSPO-PET ligand before moving to human studies. In contrast, large animal models, although more expensive, are needed since the physiology of the models better reflects the human condition and/or the imaging cannot be easily scaled up to humans if a small animal model were used. For example, most recently, Yang et al developed cardiac BOLD applications in the canine as a rodent model would not have been of value in developing cardiac BOLD for human application[61]. Translation of therapeutic interventions from rodents to humans has, in general, had a high failure rate[134]. For the development of imaging biomarkers, this problem is exacerbated by the non-linear scaling from rodent to human imaging modalities[86,135–137]. In contrast, large animal models have a reasonable translation record[138,139] and little or no issues with scaling of PET and MRI since studies use human imaging equipment. Regarding coronary artery disease and inflammation, (a) infarcted myocardium results in an increase in the distribution volume of Gd-DTPA, characteristic of permanently damaged myocardium, in dogs and humans[41,46,140–142] but the increase in the distribution volume in rats also occurs in reversibly damaged tissue[143]; (b) the time course of neutrophil and macrophage activity following AMI is similar in dogs and humans, but different in rodents[15,144–146]; (c) inflammatory cell response post-AMI has the same cell markers in humans and dogs[6,147]; and (d) the course of hemorrhage and iron precipitation following AMI is similar between humans and dogs. There has been some debate regarding the use of porcine rather than canine models for the study of the evolution of acute infarction. The presence of collateral vessels in the canine myocardium is more relevant to AMI in older humans (> 50 years of age), while the lack of collaterals in pigs provides a better model for sudden death. Since progressive heart disease following AMI is predominantly seen in older individuals, the canine model is superior imaging inflammation post-MI[148,149].

SUMMARY

Standalone myocardial post-MI MRI can provide discrimination of the three tissue types: IOT, INOT, and RT. It also can provide functional information, extent of edema, and extent of hemorrhage. It can partially track/detect inflammatory cells if they can be labeled with iron particles or ^{19}F. Standalone PET (i.e., PET/CT) can quantify inflammation with ^{18}F-FDG or TSPO-targeted tracers, but not specifically with respect to pro-inflammatory vs. the anti-inflammatory signal and, in the case of ^{18}F-FDG, requires myocardial suppression which is not always successful. Hybrid PET/MRI, even with its current state of non-optimal cardiac registration, provides a complementary story that will allow the relationship between scar formation and inflammation to be discovered as is being done in other cardiac conditions such as sarcoidosis[92,150].

To date, the primary use of hybrid PET/MRI is to perform combined PET and MRI procedures in a single procedure primarily as a tool of convenience rather than as a means of greater understanding of pathophysiological mechanisms. To achieve the latter, there are four important areas of development that are required: (a) far better registration than what is available today that does not significantly sacrifice the acquisition of PET data; (b) synchronized, simultaneous acquisition of PET and MRI where MRI must have the same flexibility as list-mode PET; (c) integration of quantitative and novel MRI techniques such as cardiac BOLD; and (d) an approach that combines the large number of PET probes and determinants of MRI contrast in novel synergistic ways (see Figure 1). This will not only be impactful with currently available PET probes but would make it possible to develop new PET probes or combined PET/MRI strategies that could quantitate and differentiate between the different inflammatory cell phenotypes. Discrimination between the pro- and anti-inflammatory processes in the three tissue types post-MI will be critical for the development of inflammatory therapies and for implementation in the individual patient.

Supplementary Material

Refer to Web version on PubMed Central for supplementary material.

Funding

Wilk, B. is supported by an Ontario Graduate scholarship and a Lawson Internal Research Fund. This work was supported in part by Ontario Research Fund RS7-021 and Canadian Foundation for Innovation No. 11358.

Abbreviations

AMI	Acute myocardial infarction
MI	Myocardial infarction
IOT	Infarcted obstructed tissue
INOT	Infarcted not obstructed tissue
RT	Remote tissue
BOLD	Blood oxygen level dependent
CEST	Chemical exchange saturation transfer
SPIO	Superparamagnetic iron oxide
TSPO	Translocator protein

References

1. Braunwald E. Shattuck lecture–cardiovascular medicine at the turn of the millennium: Triumphs, concerns, and opportunities. N Engl J Med. 1997;337:1360–9. 10.1056/NEJM199711063371906. [PubMed: 9358131]
2. Braunwald E. Research advances in heart failure: A compendium. Circ Res. 2013;113:633–45. 10.1161/CIRCRESAHA.113.302254. [PubMed: 23888056]
3. Eitel I, Kubusch K, Strohm O, Desch S, Mikami Y, De Waha S, et al. Prognostic value and determinants of a hypointense infarct core in T2-weighted cardiac magnetic resonance in acute reperfused ST-elevation-myocardial infarction. Circ Cardiovasc Imaging. 2011;4:354–62. 10.1161/CIRCIMAGING.110.960500. [PubMed: 21518773]
4. Pfeffer MA, Braunwald E. Ventricular remodeling after myocardial infarction: Experimental observations and clinical implications. Circulation. 1990;81:116–72. 10.1161/01.CIR.81.4.1161.
5. Ganame J, Messalli G, Dymarkowski S, Rademakers FE, Desmet W, Van De Werf F, et al. Impact of myocardial haemorrhage on left ventricular function and remodelling in patients with reperfused acute myocardial infarction. Eur Heart J. 2009;30:1440–9. 10.1093/eurheartj/ehp093. [PubMed: 19346229]
6. Kali A, Cokic I, Tang R, Dohnalkova A, Kovarik L, Yang HJ, et al. Persistent microvascular obstruction after myocardial infarction culminates in the confluence of ferric iron oxide crystals, proinflammatory burden, and adverse remodeling. Circ Cardiovasc Imaging. 2016;9:e004996 10.1161/CIRCIMAGING.115.004996. [PubMed: 27903536]

7. Kali A, Tang RLQ, Kumar A, Min JK, Dharmakumar R. Detection of acute reperfusion myocardial hemorrhage with cardiac MR imaging: T2 versus T2*. Radiology. 2013;269:387–95. 10.1148/radiol.13122397. [PubMed: 23847253]
8. Kali A, Kumar A, Cokic I, Tang RLQ, Tsaftaris SA, Friedrich MG, et al. Chronic manifestation of postreperfusion intramyocardial hemorrhage as regional iron deposition: A cardiovascular magnetic resonance study with ex vivo validation. Circ Cardiovasc Imaging. 2013;6:218–28. 10.1161/CIRCIMAGING.112.000133. [PubMed: 23403335]
9. Frangogiannis NG. The inflammatory response in myocardial injury, repair, and remodelling. Nat Rev Cardiol. 2014;11:255–65. 10.1038/nrcardio.2014.28. [PubMed: 24663091]
10. Weir RAP, Miller AM, Murphy GEJ, Clements S, Steedman T, Connell JMC, et al. Serum soluble ST2: A potential novel mediator in left ventricular and infarct remodeling after acute myocardial infarction. J Am Coll Cardiol. 2010;55:243–50. 10.1016/j.jacc.2009.08.047. [PubMed: 20117403]
11. Fishbein MC, Maclean D, Maroko PR. The histopathologic evolution of myocardial infarction. Chest. 1978;73:843–9. 10.1378/chest.73.6.843. [PubMed: 657859]
12. Frangogiannis NG, Smith CW, Entman ML. The inflammatory response in myocardial infarction. Cardiovasc Res. 2002;53:31–47. 10.1016/S0008-6363(01)00434-5. [PubMed: 11744011]
13. Hofmann U, Knorr S, Vogel B, Weirather J, Frey A, Ertl G, et al. Interleukin-13 deficiency aggravates healing and remodeling in male mice after experimental myocardial infarction. Circ Hear Fail. 2014;7:822–30. 10.1161/CIRCHEARTFAILURE.113.001020.
14. Chatelain P, Latour JG, Tran D, de Lorgeril M, Dupras G, Bourassa M. Neutrophil accumulation in experimental myocardial infarcts: Relation with extent of injury and effect of reperfusion. Circulation. 1987;75:1083–90. 10.1161/01.CIR.75.5.1083. [PubMed: 3568308]
15. Dewald O, Ren G, Duerr GD, Zoerlein M, Klemm C, Gersch C, et al. Of mice and dogs: Species-specific differences in the inflammatory response following myocardial infarction. Am J Pathol. 2004;164:665–77. 10.1016/S0002-9440(10)63154-9. [PubMed: 14742270]
16. Epelman S, Lavine KJ, Randolph GJ. Origin and functions of tissue macrophages. Immunity. 2014;41:21–35. 10.1016/j.immuni.2014.06.013. [PubMed: 25035951]
17. Lavine KJ, Epelman S, Uchida K, Weber KJ, Nichols CG, Schilling JD, et al. Distinct macrophage lineages contribute to disparate patterns of cardiac recovery and remodeling in the neonatal and adult heart. Proc Natl Acad Sci. 2014;111:16029–34. 10.1073/pnas.1406508111. [PubMed: 25349429]
18. Serhan CN, Savill J. Resolution of inflammation: The beginning programs the end. Nat Immunol. 2005;6:1191–7. 10.1038/ni1276. [PubMed: 16369558]
19. Warnatsch A, Ioannou M, Wang Q, Papayannopoulos V. Neutrophil extracellular traps license macrophages for cytokine production in atherosclerosis. Science. 2015;349:316–20. 10.1126/science.aaa8064. [PubMed: 26185250]
20. Yan Y, Gause KT, Kamphuis MMJ, Ang CS, O'Brien-Simpson NM, Lenzo JC, et al. Differential roles of the protein corona in the cellular uptake of nanoporous polymer particles by monocyte and macrophage cell lines. ACS Nano. 2013;7:10960–70. 10.1021/nn404481f. [PubMed: 24256422]
21. Bronte V, Pittet MJ. The spleen in local and systemic regulation of immunity. Immunity. 2013;39:806–18. 10.1016/j.immuni.2013.10.010. [PubMed: 24238338]
22. Swirski FK, Nahrendorf M, Etzrodt M, Wildgruber M, Cortez-Retamozo V, Panizzi P, et al. Identification of splenic reservoir monocytes and their deployment to inflammatory sites. Science. 2009;325:612–6. 10.1126/science.1175202. [PubMed: 19644120]
23. Dutta P, Nahrendorf M. Monocytes in myocardial infarction. Arterioscler Thromb Vasc Biol. 2015;35:1066–70. 10.1161/ATVBAHA.114.304652. [PubMed: 25792449]
24. Hettinger J, Richards DM, Hansson J, Barra MM, Joschko AC, Krijgsveld J, et al. Origin of monocytes and macrophages in a committed progenitor. Nat Immunol. 2013;14:821–30. 10.1038/ni.2638. [PubMed: 23812096]
25. Koelwyn GJ, Corr EM, Erbay E, Moore KJ. Regulation of macrophage immunometabolism in atherosclerosis. Nat Immunol. 2018;19:526–37. 10.1038/s41590-018-0113-3. [PubMed: 29777212]

26. Tavakoli S, Zamora D, Ullevig S, Asmis R. Bioenergetic profiles diverge during macrophage polarization: Implications for the interpretation of 18F-FDG PET imaging of atherosclerosis. J Nucl Med. 2013;54:1661–7. 10.2967/jnumed.112.119099. [PubMed: 23886729]
27. Dobaczewski M, Xia Y, Bujak M, Gonzalez-Quesada C, Frangogiannis NG. CCR5 signaling suppresses inflammation and reduces adverse remodeling of the infarcted heart, mediating recruitment of regulatory T cells. Am J Pathol. 2010;176:2177–87. 10.2353/ajpath.2010.090759. [PubMed: 20382703]
28. Frangogiannis NG. Regulation of the inflammatory response in cardiac repair. Circ Res. 2012;110:159–73. 10.1161/CIRCRESAHA.111.243162. [PubMed: 22223212]
29. Seropian IM, Toldo S, Van Tassell BW, Abbate A. Anti-inflammatory strategies for ventricular remodeling following St-segment elevation acute myocardial infarction. J Am Coll Cardiol. 2014;63:1593–603. 10.1016/j.jacc.2014.01.014. [PubMed: 24530674]
30. Satomi T, Ogawa M, Mori I, Ishino S, Kubo K, Magata Y, et al. Comparison of contrast agents for atherosclerosis imaging using cultured macrophages: FDG versus ultrasmall superparamagnetic iron oxide. J Nucl Med. 2013;54:999–1004. 10.2967/jnumed.112.110551. [PubMed: 23670898]
31. Zhu L, Zhao Q, Yang T, Ding W, Zhao Y. Cellular metabolism and macrophage functional polarization. Int Rev Immunol. 2015;34:82–100. 10.3109/08830185.2014.969421. [PubMed: 25340307]
32. Recalcati S, Locati M, Marini A, Santambrogio P, Zaninotto F, De Pizzol M, et al. Differential regulation of iron homeostasis during human macrophage polarized activation. Eur J Immunol. 2010;40:824–35. 10.1002/eji.200939889. [PubMed: 20039303]
33. Corna G, Campana L, Pignatti E, Castiglioni A, Tagliafico E, Bosurgi L, et al. Polarization dictates iron handling by inflammatory and alternatively activated macrophages. Haematologica. 2010;95:1814–22. 10.3324/haematol.2010.023879. [PubMed: 20511666]
34. Goldhawk D, Gelman N, Sengupta A, Prato F. The interface between iron metabolism and gene-based iron contrast for MRI. Magn Reson Insights. 2015;8:9–14. 10.4137/mri.s23555. [PubMed: 26483608]
35. Young AA, Kramer CM, Ferrari VA, Axel L, Reichek N. Three-dimensional left ventricular deformation in hypertrophic cardiomyopathy. Circulation. 1994;90:854–67. 10.1161/01.CIR.90.2.854. [PubMed: 8044957]
36. Everaars H, Robbers LFHJ, Götte M, Croisille P, Hirsch A, Teunissen PFA, et al. Strain analysis is superior to wall thickening in discriminating between infarcted myocardium with and without microvascular obstruction. Eur Radiol. 2018;28:5171–81. 10.1007/s00330-018-5493-0. [PubMed: 29948065]
37. Lotz J, Meier C, Leppert A, Galanski M. Cardiovascular flow measurement with imaging: Basic facts and implementation. RadioGraphics. 2002;22:651–71. [PubMed: 12006694]
38. Vasanawala SS, Hanneman K, Alley MT, Hsiao A. Congenital heart disease assessment with 4D flow MRI. J Magn Reson Imaging. 2015;42:870–86. 10.1002/jmri.24856. [PubMed: 25708923]
39. Garcia J, Sheitt H, Bristow MS, Lydell C, Howarth AG, Heydari B, et al. Left atrial vortex size and velocity distributions by 4D flow MRI in patients with paroxysmal atrial fibrillation: Associations with age and CHA2 DS2-VASc risk score. J Magn Reson Imaging. 2019 10.1002/jmri.26876.
40. Thornhill RE, Prato FS, Pereira RS, Wisenberg G, Sykes J. Examining a canine model of stunned myocardium with Gd-DTPA-enhanced MRI. Magn Reson Med. 2001;45:864–71. 10.1002/mrm.1115. [PubMed: 11323813]
41. Thornhill RE, Prato FS, Wisenberg G, White JA, Nowell J, Sauer A. Feasibility of the single-bolus strategy for measuring the partition coefficient of Gd-DTPA in patients with myocardial infarction: Independence of image delay time and maturity of scar. Magn Reson Med. 2006;55:780–9. 10.1002/mrm.20830. [PubMed: 16508912]
42. Pereira RS, Prato FS, Sykes J, Wisenberg G. Assessment of myocardial viability using MRI during a constant infusion of GD-DTPA: Further studies at early and late periods of reperfusion. Magn Reson Med. 1999;42:60–8. 10.1002/(SICI)1522-2594(199907)42:1<60:AID-MRM10>3.0.CO;2-9. [PubMed: 10398951]

43. Flacke SJ, Fischer SE. Measurement of the gadopentetate dimeglumine partition coefficient in human myocardium in vivo: Normal distribution and elevation in acute and chronic infarction. Radiology. 2001;218:703–10. [PubMed: 11230643]
44. Kim RJ, Fieno DS, Parrish TB, Harris K, Chen EL, Simonetti O, et al. Relationship of MRI delayed contrast enhancement to irreversible injury, infarct age, and contractile function. Circulation. 1999;100:1992–2002. 10.1161/01.CIR.100.19.1992. [PubMed: 10556226]
45. Lekx KS, Prato FS, Sykes J, Wisenberg G. The partition coefficient of Gd-DTPA reflects maintained tissue viability in a canine model of chronic significant coronary stenosis. J Cardiovasc Magn Reson. 2004;6:33–42. 10.1081/JCMR-120027803. [PubMed: 15054927]
46. Pereira RS, Wisenberg G, Prato FS, Yvorchuk K. Clinical assessment of myocardial viability using MRI during a constant infusion of Gd-DTPA. Magn Reson Mater Physics, Biol Med. 2000;11:104–13. 10.1016/S1352-8661(00)00093-4.
47. Wu KC, Heldman AW, Brinker JA, Hare JM, Lima JAC. Microvascular obstruction after nonsurgical septal reduction for the treatment of hypertrophic cardiomyopathy. Circulation. 2001;104:1868 10.1161/hc4001.096355. [PubMed: 11591628]
48. Kim RJ, Wu E, Rafael A, Chen EL, Parker MA, Simonetti O, et al. The use of contrast-enhanced magnetic resonance imaging to identify reversible myocardial dysfunction. N Engl J Med. 2000;343:1445–53. 10.1016/s1062-1458(01)00166-0. [PubMed: 11078769]
49. Kali A, Cokic I, Tang RLQ, Yang HJ, Sharif B, Marbán E, et al. Determination of location, size, and transmurality of chronic myocardial infarction without exogenous contrast media by using cardiac magnetic resonance imaging at 3 T. Circ Cardiovasc Imaging. 2014;7:471–81. 10.1161/CIRCIMAGING.113.001541. [PubMed: 24682268]
50. Kali A, Choi EY, Sharif B, Kim YJ, Bi X, Spottiswoode B, et al. Native T1 mapping by 3-T CMR imaging for characterization of chronic myocardial infarctions. JACC Cardiovasc Imaging. 2015;8:1019–30. 10.1016/j.jcmg.2015.04.018. [PubMed: 26298071]
51. Wang G, Yang H-J, Kali A, Cokic I, Tang R, Xie G, et al. Influence of myocardial hemorrhage on staging of reperfused myocardial infarctions with T2 cardiac magnetic resonance imaging. JACC Cardiovasc Imaging. 2019;12:693–703. 10.1016/j.jcmg.2018.01.018. [PubMed: 29680356]
52. Jerosch-Herold M, Seethamraju RT, Swingen CM, Wilke NM, Stillman AE. Analysis of myocardial perfusion MRI. J Magn Reson Imaging. 2004;19:758–70. 10.1002/jmri.20065. [PubMed: 15170782]
53. Bellamy DD, Pereira RS, McKenzie CA, Prato FS, Drost DJ, Sykes J, et al. Gd-DTPA bolus tracking in the myocardium using T1 fast acquisition relaxation mapping (T1 FARM). Magn Reson Med. 2001;46:555–64. 10.1002/mrm.1227. [PubMed: 11550249]
54. Ishida M, Schuster A, Morton G, Chiribiri A, Hussain S, Paul M, et al. Development of a universal dual-bolus injection scheme for the quantitative assessment of myocardial perfusion cardiovascular magnetic resonance. J Cardiovasc Magn Reson. 2011;13:28 10.1186/1532-429X-13-28x. [PubMed: 21609423]
55. Papanastasiou G, Williams MC, Kershaw LE, Dweck MR, Alam S, Mirsadraee S, et al. Measurement of myocardial blood flow by cardiovascular magnetic resonance perfusion: Comparison of distributed parameter and Fermi models with single and dual bolus. J Cardiovasc Magn Reson. 2015 10.1186/s12968-015-0125-1.
56. Tong CY, Prato FS, Wisenberg G, Lee TY, Carroll E, Sandler D, et al. Measurement of the extraction efficiency and distribution volume for Gd-DTPA in normal and diseased canine myocardium. Magn Reson Med. 1993;30:337–46. 10.1002/mrm.1910300310. [PubMed: 8412605]
57. Maddahi J, Packard RRS. Cardiac PET perfusion tracers: Current status and future directions. Semin Nucl Med. 2014;44:333–43. 10.1053/j.semnuclmed.2014.06.011. [PubMed: 25234078]
58. Kunze KP, Rischpler C, Hayes C, Ibrahim T, Laugwitz KL, Haase A, et al. Measurement of extracellular volume and transit time heterogeneity using contrast enhanced myocardial perfusion MRI in patients after acute myocardial infarction. Magn Reson Med. 2017;77:2320–30. 10.1002/mrm.26320. [PubMed: 27364875]
59. Schelbert HR, Phelps ME, Huang SC, MacDonald NS, Hansen H, Selin C, et al. N-13 ammonia as an indicator of myocardial blood flow. Circulation. 1981;63:1259–72. 10.1161/01.CIR.63.6.1259. [PubMed: 7226473]

60. Li D, Dhawale P, Rubin PJ, Haacke EM, Gropler RJ. Myocardial signal response to dipyridamole and dobutamine: Demonstration of the BOLD effect using a doubleecho gradient-echo sequence. Magn Reson Med. 1996;36:16–20. 10.1002/mrm.1910360105. [PubMed: 8795015]

61. Yang H-J, Ilkary O, Dey D, Sykes J, Klein M, Butler J, et al. Accurate needle-free assessment of myocardial oxygenation for ischemic heart disease. Sci Transl Med. 2019;11:eaat4407. [PubMed: 31142677]

62. Van Zijl PCM, Yadav NN. Chemical exchange saturation transfer (CEST): What is in a name and what isn't ? Magn Reson Med. 2011;65:927–48. 10.1002/mrm.22761. [PubMed: 21337419]

63. Liu G, Song X, Chan KWY, McMahon MT. Nuts and bolts of chemical exchange saturation transfer MRI. NMR Biomed. 2013;26:810–28. 10.1002/nbm.2899. [PubMed: 23303716]

64. Vinogradov E, Sherry AD, Lenkinski RE. CEST: From basic principles to applications, challenges and opportunities. J Magn Reson. 2013;229:155–72. 10.1016/j.jmr.2012.11.024. [PubMed: 23273841]

65. Jones CK, Schlosser MJ, Van Zijl PCM, Pomper MG, Golay X, Zhou J. Amide proton transfer imaging of human brain tumors at 3T. Magn Reson Med. 2006;56:585–92. 10.1002/mrm.20989. [PubMed: 16892186]

66. Cai K, Haris M, Singh A, Kogan F, Greenberg JH, Hariharan H, et al. Magnetic resonance imaging of glutamate. Nat Med. 2012;18:302–6. 10.1038/nm.2615. [PubMed: 22270722]

67. Haris M, Nanga RRPR, Singh A, Cai K, Kogan F, Hariharan H, et al. Exchange rates of creatine kinase metabolites: Feasibility of imaging creatine by chemical exchange saturation transfer MRI. NMR Biomed. 2013;25:1305–9. 10.1002/nbm.2792.Exchange.

68. Lindeman LR, Randtke EA, High RA, Jones KM, Howison CM, Pagel MD. A comparison of exogenous and endogenous CEST MRI methods for evaluating in vivo pH. Magn Reson Med. 2018;79:2766–72. 10.1002/mrm.26924. [PubMed: 29024066]

69. Jones KM, Randtke EA, Yoshimaru ES, Howison CM, Chalasani P, Klein RR, et al. Clinical translation of tumor acidosis measurements with AcidoCEST MRI. Mol Imaging Biol. 2017;19:617–25. 10.1007/s11307-016-1029-7. [PubMed: 27896628]

70. Chan KWY, McMahon MT, Kato Y, Liu G, Bulte JWM, Bhujwalla ZM, et al. Natural D-glucose as a biodegradable MRI contrast agent for detecting cancer. Magn Reson Med. 2012;68:1764–73. 10.1002/mrm.24520. [PubMed: 23074027]

71. Walker-Samuel S, Ramasawmy R, Torrealdea F, Rega M, Rajkumar V, Johnson SP, et al. In vivo imaging of glucose uptake and metabolism in tumors. Nat Med. 2013;19:1067–72. 10.1038/nm.3252. [PubMed: 23832090]

72. Rivlin M, Horev J, Tsarfaty I, Navon G. Molecular imaging of tumors and metastases using chemical exchange saturation transfer (CEST) MRI. Sci Rep. 2013;3:3045 10.1038/srep03045. [PubMed: 24157711]

73. Jones KM, Pollard AC, Pagel MD. Clinical applications of chemical exchange saturation transfer (CEST) MRI. J Magn Reson Imaging. 2018;47:11–27. 10.1002/jmri.25838. [PubMed: 28792646]

74. Haris M, Singh A, Cai K, Kogan F, McGarvey J, Debrosse C, et al. A technique for in vivo mapping of myocardial creatine kinase metabolism. Nat Med. 2014;20:209–14. 10.1038/nm.3436. [PubMed: 24412924]

75. Zhou Z, Nguyen C, Chen Y, Shaw JL, Deng Z, Xie Y, et al. Optimized CEST cardiovascular magnetic resonance for assessment of metabolic activity in the heart. J Cardiovasc Magn Reson. 2017;19:95 10.1186/s12968-017-0411-1. [PubMed: 29191206]

76. Pumphrey A, Yang Z, Ye S, Powell DK, Thalman S, Watt DS, et al. Advanced cardiac chemical exchange saturation transfer (cardioCEST) MRI for in vivo cell tracking and metabolic imaging. NMR Biomed. 2016;29:74–83. 10.1002/nbm.3451. [PubMed: 26684053]

77. Petz A, Grandoch M, Gorski DJ, Abrams M, Piroth MA, Schneckmann R, et al. Cardiac hyaluronan synthesis is critically involved in the cardiac macrophage response and promotes healing after ischemia reperfusion injury. Circ Res. 2019;124:1433–47. 10.1161/CIRCRESAHA.118.313285. [PubMed: 30916618]

78. Bulte JWM, Daldrup-Link HE. Clinical tracking of cell transfer and cell transplantation: Trials and tribulations. Radiology. 2018 10.1148/radiol.2018180449.

79. Suzuki Y, Cunningham CH, Noguchi KI, Chen IY, Weissman IL, Yeung AC, et al. In vivo serial evaluation of superparamagnetic iron-oxide labeled stem cells by off resonance positive contrast. Magn Reson Med. 2008;60:1269–75. 10.1002/mrm.21816. [PubMed: 19030159]

80. Makela AV, Foster PJ. Imaging macrophage distribution and density in mammary tumors and lung metastases using fluorine-19 MRI cell tracking. Magn Reson Med. 2018;80:1138–47. 10.1002/mrm.27081. [PubMed: 29327789]

81. Rothe M, Jahn A, Weiss K, Hwang JH, Szendroedi J, Kelm M, et al. In vivo 19 F MR inflammation imaging after myocardial infarction in a large animal model at 3 T. Magn Reson Mater Physics, Biol Med. 2019;32:5–13. 10.1007/s10334-018-0714-8.

82. Bönner F, Merx MW, Klingel K, Begovatz P, Flögel U, Sager M, et al. Monocyte imaging after myocardial infarction with ^{19}FMRI at 3 T: A pilot study in explanted porcine hearts. Eur Heart J Cardiovasc Imaging. 2015;16:612–20. 10.1093/ehjci/jev008. [PubMed: 25733209]

83. Dassanayake PSB, Goldhawk DE. Monocyte MRI relaxation rates are regulated by extracellular iron and hepcidin MSc Thesis, West University; 2019

84. Liu L, Alizadeh K, Donnelly SC, Dassanayake P, Hou TT, McGirr R, et al. MagA expression attenuates iron export activity in undifferentiated multipotent P19 cells. PLoS ONE. 2019;14:1–19. 10.1371/journal.pone.0217842.

85. Yang HJ, Sharif B, Pang J, Kali A, Bi X, Cokic I, et al. Free-breathing, motioncorrected, highly efficient whole heart T2 mapping at 3T with hybrid radial-cartesian trajectory. Magn Reson Med. 2016;75:126–36. 10.1002/mrm.25576. [PubMed: 25753385]

86. Goldhawk DE, Rohani R, Sengupta A, Gelman N, Prato FS. Using the magnetosome to model effective gene-based contrast for magnetic resonance imaging. Wiley Interdiscip Rev Nanomed Nanobiotechnol. 2012;4:378–88. 10.1002/wnan.1165. [PubMed: 22407727]

87. Goldhawk DE, Gelman N, Thompson RT, Prato FS. Forming magnetosome-like nanoparticles in mammalian cells for molecular MRI. In: Design and applications of nanoparticles in biomedical imaging; 2017 p. 187–203

88. Ylä-Herttuala S, Baker AH. Cardiovascular gene therapy: Past, present, and future. Mol Ther. 2017;25:1095–106. 10.1016/j.ymthe.2017.03.027. [PubMed: 28389321]

89. Wollenweber T, Bengel FM. Cardiac molecular imaging. Semin Nucl Med. 2014;44:386–97. 10.1053/j.semnuclmed.2014.05.002. [PubMed: 25234082]

90. Larson SR, Pieper JA, Hulten EA, Ficaro EP, Corbett JR, Murthy VL, et al. Characterization of a highly effective preparation for suppression of myocardial glucose utilization. J Nucl Cardiol. 2019 10.1007/s12350-019-01786-w.

91. Borchert T, Beitar L, Langer LBN, Polyak A, Wester H-J, Ross TL, et al. Dissecting the target leukocyte subpopulations of clinically relevant inflammation radiopharmaceuticals. J Nucl Cardiol. 2019 10.1007/s12350-019-01929-z.

92. Wisenberg G, Thiessen JD, Pavlovsky W, Butler J, Wilk B, Prato FS. Same day comparison of PET/CT and PET/MR in patients with cardiac sarcoidosis. J Nucl Cardiol. 2019 10.1007/s12350-018-01578-8.

93. Murthy VL, Bateman TM, Beanlands RS, Berman DS, Borges-Neto S, Chareonthaitawee P, et al. Clinical quantification of myocardial blood flow using PET: Joint position paper of the SNMMI cardiovascular council and the ASNC. J Nucl Med. 2018;59:273–93. 10.2967/jnumed.117.201368. [PubMed: 29242396]

94. Rust TC, DiBella EVR, McGann CJ, Christian PE, Hoffman JM, Kadrmas DJ. Rapid dual-injection single-scan 13N-ammonia PET for quantification of rest and stress myocardial blood flows. Phys Med Biol. 2006;51:5347–62. 10.1088/0031-9155/51/20/018. [PubMed: 17019043]

95. Ory D, Celen S, Verbruggen A, Bormans G. PET radioligands for in vivo visualization of neuroinflammation. Curr Pharm Des. 2014;20:5897–913. 10.2174/1381612820666140613120212. [PubMed: 24939192]

96. Vivash L, OBrien TJ. Imaging microglial activation with TSPO PET: Lighting up neurologic diseases? J Nucl Med. 2015;57:165–8. 10.2967/jnumed.114.141713. [PubMed: 26697963]

97. Thackeray JT, Hupe HC, Wang Y, Bankstahl JP, Berding G, Ross TL, et al. Myocardial inflammation predicts remodeling and neuroinflammation after myocardial infarction. J Am Coll Cardiol. 2018;71:263–75. 10.1016/j.jacc.2017.11.024. [PubMed: 29348018]

98. Van De Wiele C, Sathekge M, Maes A. Targeting monocytes and macrophages by means of SPECT and PET. Q J Nucl Med Mol Imaging. 2014;58:269–75. [PubMed: 24844256]

99. Bansal A, Pandey MK, Demirhan YE, Nesbitt JJ, Crespo-Diaz RJ, Terzic A, et al. Novel 89Zr cell labeling approach for PET-based cell trafficking studies. EJNMMI Res. 2015 10.1186/s13550-015-0098-y.

100. Prato FS, Butler J, Sykes J, Keenliside L, Blackwood KJ, Thompson RT, et al. Can the inflammatory response be evaluated using 18F-FDG within zones of microvascular obstruction after myocardial infarction? J Nucl Med. 2015;56:299–304. 10.2967/jnumed.114.147835. [PubMed: 25572090]

101. Blackwood KJ, Lewden B, Wells RG, Sykes J, Stodilka RZ, Wisenberg G, et al. In vivo SPECT quantification of transplanted cell survival after engraftment using 111In-tropolone in infarcted canine myocardium. J Nucl Med. 2009;50:927–35. 10.2967/jnumed.108.058966. [PubMed: 19470852]

102. Amsalem Y, Mardor Y, Feinberg MS, Landa N, Miller L, Daniels D, et al. Iron-oxide labeling and outcome of transplanted mesenchymal stem cells in the infarcted myocardium. Circulation. 2007;116:38–45. 10.1161/CIRCULATIONAHA.106.680231.

103. Yao Y, Li Y, Ma G, Liu N, Ju S, Jin J, et al. In vivo magnetic resonance imaging of injected endothelial progenitor cells after myocardial infarction in rats. Mol Imaging Biol. 2011;13:303–13. 10.1007/s11307-010-0359-0. [PubMed: 20552286]

104. Parashurama N, Ahn BC, Ziv K, Ito K, Paulmurugan R, Will-mann JK, et al. Multimodality molecular imaging of cardiac cell transplantation: Part I Reporter gene design, characterization, and optical in vivo imaging of bone marrow stromal cells after myocardial infarction. Radiology. 2016;280:815–25. 10.1148/radiol.2016140049. [PubMed: 27308957]

105. Miyagawa M, Anton M, Haubner R, Simoes MV, Städele C, Erhardt W, et al. PET of cardiac transgene expression: comparison of 2 approaches based on herpesviral thymidine kinase reporter gene. J Nucl Med. 2004;45:1917–23. [PubMed: 15534063]

106. Rausch I, Quick HH, Cal-Gonzalez J, Sattler B, Boellaard R, Beyer T. Technical and instrumentational foundations of PET/MRI. Eur J Radiol. 2017;94:A3–13. 10.1016/j.ejrad.2017.04.004. [PubMed: 28431784]

107. Farag A, Thompson RT, Thiessen JD, Butler J, Prato FS, Théberge J. Assessment of a novel 32-channel phased array for cardiovascular hybrid PET/MRI imaging: MRI performance. Eur J Hybrid Imaging. 2019 10.1186/s41824-019-0061-7.

108. Vontobel J, Liga R, Possner M, Clerc OF, Mikulicic F, Veit-Haibach P, et al. MRbased attenuation correction for cardiac FDG PET on a hybrid PET/MRI scanner: comparison with standard CT attenuation correction. Eur J Nucl Med Mol Imaging. 2015;42:1574–80. 10.1007/s00259-015-3089-3. [PubMed: 26091704]

109. Lau JMC, Laforest R, Sotoudeh H, Nie X, Sharma S, McConathy J, et al. Evaluation of attenuation correction in cardiac PET using PET/MR. J Nucl Cardiol. 2017;24:839–46. 10.1007/s12350-015-0197-1. [PubMed: 26499770]

110. Lewis CE, Prato FS, Drost DJ, Nicholson RL. Comparison of respiratory triggering and gating techniques for the removal of respiratory artifacts in MR imaging. Radiology. 1986;160:803–10. 10.1148/radiology.160.3.3737921. [PubMed: 3737921]

111. Pang J, Bhat H, Sharif B, Fan Z, Thomson LEJ, Labounty T, et al. Whole-heart coronary MRA with 100% respiratory gating efficiency: Self-navigated threedimensional retrospective image-based motion correction (TRIM). Magn Reson Med. 2014;71:67–74. 10.1002/mrm.24628. [PubMed: 23401157]

112. Kolbitsch C, Ahlman MA, Davies-Venn C, Evers R, Hansen M, Peressutti D, et al. Cardiac and respiratory motion correction for simultaneous cardiac PET/MR. J Nucl Med. 2017;58:846–52. 10.2967/jnumed.115.171728. [PubMed: 28183991]

113. Munoz C, Neji R, Kunze KP, Nekolla SG, Botnar RM, Prieto C. Respiratory- and cardiac motion-corrected simultaneous wholeheart PET and dual phase coronary MR angiography. Magn Reson Med. 2019;81:1671–84. 10.1002/mrm.27517. [PubMed: 30320931]

114. Feng T, Wang J, Tsui BMW. Dual respiratory and cardiac motion estimation in PET imaging: Methods design and quantitative evaluation. Med Phys. 2018;45:1481–90. 10.1002/mp.12793. [PubMed: 29405313]

115. Robson PM, Trivieri MG, Karakatsanis NA, Padilla M, Abgral R, Dweck MR, et al. Correction of respiratory and cardiac motion in cardiac PET/MR using MR-based motion modeling. Phys Med Biol. 2018;63:225011 10.1088/1361-6560/aaea97. [PubMed: 30426968]

116. Petibon Y, Sun T, Han PK, Ma C, El Fakhri G, Ouyang J. MR-based cardiac and respiratory motion correction of PET: Application to static and dynamic cardiac 18FFDG imaging. Phys Med Biol. 2019;64:195009 10.1088/1361-6560/ab39c2. [PubMed: 31394518]

117. Klyuzhin IS, Sossi V. PET image reconstruction and deformable motion correction using unorganized point clouds. IEEE Trans Med Imaging. 2017;36:1263–75. 10.1109/TMI.2017.2675989. [PubMed: 28287962]

118. Berg E, Gill H, Marik J, Ogasawara A, Williams SP, van Dongen GAMS, et al. Totalbody PET and highly stable chelators together enable meaningful 89 Zr-antibody-PET studies up to 30 days post-injection. J Nucl Med. 2019 10.2967/jnumed.119.230961.

119. Barton GP, Vildberg L, Goss K, Aggarwal N, Eldridge M, McMillan AB. Simultaneous determination of dynamic cardiac metabolism and function using PET/MRI. J Nucl Cardiol. 2018 10.1007/s12350-018-1287-7.

120. Wilk B, Wisenberg G, Sykes J, Butler J, Kovacs MS, Thompson RT, et al. Quantifying inflammation in infarcted myocardial tissue with severely reduced flow: A hybrid PET/MRI approach using a prolonged constant infusion of 18F-FDG and Gd-DTPA. In: Society of Nuclear Medicine and Molecular Imaging 2018 annual meet; 2018

121. Kunze KP, Nekolla SG, Rischpler C, Zhang SHL, Hayes C, Langwieser N, et al. Myocardial perfusion quantification using simultaneously acquired 13NH3- ammonia PET and dynamic contrast-enhanced MRI in patients at rest and stress. Magn Reson Med. 2018 10.1002/mrm.27213.

122. Feng L, Grimm R, Block KT, Chandarana H, Kim S, Xu J, et al. Golden-angle radial sparse parallel MRI: Combination of compressed sensing, parallel imaging, and golden-angle radial sampling for fast and flexible dynamic volumetric MRI. Magn Reson Med. 2014;72:707–17. 10.1002/mrm.24980. [PubMed: 24142845]

123. Piekarski E, Chitiboi T, Ramb R, Feng L, Axel L. Use of self-gated radial cardiovascular magnetic resonance to detect and classify arrhythmias (atrial fibrillation and premature ventricular contraction). J Cardiovasc Magn Reson. 2016;18:83 10.1186/s12968-016-0306-6. [PubMed: 27884152]

124. Piekarski E, Chitiboi T, Ramb R, Latson LA, Bhatla P, Feng L, et al. Two-dimensional XD-GRASP provides better image quality than conventional 2D cardiac cine MRI for patients who cannot suspend respiration. Magn Reson Mater Phys Biol Med. 2018;31:49–59. 10.1007/s10334-017-0655-7.

125. Piccini D, Feng L, Bonanno G, Coppo S, Yerly J, Lim RP, et al. Four-dimensional respiratory motion-resolved whole heart coronary MR angiography. Magn Reson Med. 2017;77:1473–84. 10.1002/mrm.26221. [PubMed: 27052418]

126. Heydari B, Kwong RY, Jerosch-Herold M. Technical advances and clinical applications of quantitative myocardial blood flow imaging with cardiac MRI. Prog Cardiovasc Dis. 2015;57:615–22. 10.1016/j.pcad.2015.02.003. [PubMed: 25727176]

127. Yang H-J, Christodoulou AG, Sykes J, Bi X, Cokic I, Prato FS, et al. Beat-by-beat dynamic assessment of myocardial oxygenation with highly time-resolved free breathing, ungated cardiac T2 BOLD MRI using a low-rank tensor formulation. In: International Society of Magnetic Resonance in Medicine 2018 annual meet; 2018

128. Davidson CQ, Phenix CP, Tai T, Khaper N, Lees SJ. Searching for novel PET radiotracers: Imaging cardiac perfusion, metabolism and inflammation. Am J Nucl Med Mol Imaging. 2018;8:200–27. [PubMed: 30042871]

129. Tofts PS. Modeling tracer kinetics in dynamic Gd-DTPA MR imaging. J Magn Reson Imaging. 1997;7:91–101. 10.1002/jmri.1880070113. [PubMed: 9039598]

130. Richard MA, Fouquet JP, Lebel R, Lepage M. MRI-guided derivation of the input function for PET kinetic modeling. PET Clin. 2016;11:193–202. 10.1016/j.cpet.2015.09.003. [PubMed: 26952731]
131. Qi Q, Fox MS, Bartha R, Hoffman L, Lee TY, Thiessen JD. Comparison of glucose-CEST with perfusion and glycolysis measurements in a C6 rat model of glioma. In: World molecular imaging congress 2018; 2018
132. Dey D, Slomka PJ, Leeson P, Comaniciu D, Shrestha S, Sengupta PP, et al. Artificial intelligence in cardiovascular imaging. J Am Coll Cardiol. 2019;73:1317–35. 10.1016/j.jacc.2018.12.054. [PubMed: 30898208]
133. Tan LK, McLaughlin RA, Lim E, Abdul Aziz YF, Liew YM. Fully automated segmentation of the left ventricle in cine cardiac MRI using neural network regression. J Magn Reson Imaging. 2018;48:140–52. 10.1002/jmri.25932. [PubMed: 29316024]
134. Couzin-Frankel J. When mice mislead. Science. 2013;342:922–3. 10.1126/science.342.6161.922. [PubMed: 24264972]
135. Gore JC, Yankeelov TE, Peterson TE, Avison MJ. Molecular imaging without radiopharmaceuticals? J Nucl Med. 2009;50:999–1007. 10.2967/jnumed.108.059576. [PubMed: 19443583]
136. Meikle SR, Kench P, Kassiou M, Banati RB. Small animal SPECT and its place in the matrix of molecular imaging technologies. Phys Med Biol. 2005;50:R45–61. 10.1088/0031-9155/50/22/R01. [PubMed: 16264248]
137. Moses WW. Fundamental limits of spatial resolution in PET. Nucl Instruments Methods Phys Res Sect A. 2011;648:S236–40. 10.1016/j.nima.2010.11.092.
138. Grimm D. From bark to bedside. Science. 2016;353:638–40. 10.1126/science.353.6300.638. [PubMed: 27516580]
139. Thompson K, Wisenberg G, Sykes J, Terry Thompson R. MRI/MRS evaluation of cariporide in a canine long-term model of reperfused ischemic insults. J Magn Reson Imaging. 2003;17:136–41. 10.1002/jmri.10222. [PubMed: 12500283]
140. Diesbourg LD, Prato FS, Wisenberg G, Drost DJ, Marshall TP, Carroll SE, et al. Quantification of myocardial blood flow and extracellular volumes using a bolus injection of Gd-DTPA: Kinetic modeling in canine ischemic disease. Magn Reson Med. 1992;23:239–53. 10.1002/mrm.1910230205. [PubMed: 1549039]
141. Thornhill RE, Prato FS, Wisenberg G. The assessment of myocardial viability: A review of current diagnostic imaging approaches. J Cardiovasc Magn Reson. 2002;4:381–410. 10.1081/jcmr-120013301. [PubMed: 12234110]
142. Weinsaft JW, Klem I, Judd RM. MRI for the assessment of myocardial viability. Magn Reson Imaging Clin N Am. 2007;25:35–6. 10.1016/j.mric.2007.08.007.
143. Saeed M, Lund G, Wendland MF, Bremerich J, Weinmann HJ, Higgins CB. Magnetic resonance characterization of the periinfarction zone of reperfused myocardial infarction with necrosis-specific and extracellular nonspecific contrast media. Circulation. 2001;103:871–6. 10.1161/01.CIR.103.6.871. [PubMed: 11171797]
144. Frangogiannis NG, Mendoza LH, Ren G, Akrivakis S, Jackson PL, Michael LH, et al. MCSF expression is induced in healing myocardial infarcts and may regulate monocyte and endothelial cell phenotype. Am J Physiol Circ Physiol. 2003;285:H483–92. 10.1152/ajpheart.01016.2002.
145. Frantz S, Nahrendorf M. Cardiac macrophages and their role in ischaemic heart disease. Cardiovasc Res. 2014;102:240–8. 10.1093/cvr/cvu025. [PubMed: 24501331]
146. Lee WW, Marinelli B, Van Der Laan AM, Sena BF, Gorbatov R, Leuschner F, et al. PET/MRI of inflammation in myocardial infarction. J Am Coll Cardiol. 2012;59:153–63. 10.1016/j.jacc.2011.08.066. [PubMed: 22222080]
147. Hamirani YS, Wong A, Kramer CM, Salerno M. Effect of microvascular obstruction and intramyocardial hemorrhage by CMR on LV remodeling and outcomes after myocardial infarction: A systematic review and meta-analysis. JACC Cardiovasc Imaging. 2014;7:940–52. 10.1016/j.jcmg.2014.06.012. [PubMed: 25212800]
148. Maxwell MP, Hearse DJ, Yellon DM. Species variation in the coronary collateral circulation during regional myocardial ischaemia: A critical determinant of the rate of evolution and extent

of myocardial infarction. Cardiovasc Res. 1987;21:737–46. 10.1093/cvr/21.10.737. [PubMed: 3440266]

149. Phelps ME, Huang SC, Hoffman EJ, Selin C, Sokoloff L, Kuhl DE. Tomographic measurement of local cerebral glucose metabolic rate in humans with (F-18)2-fluoro-2-deoxy-d-glucose: Validation of method. Ann Neurol. 1979;6:371–88. 10.1002/ana.410060502. [PubMed: 117743]
150. Dweck MR, Abgral R, Trivieri MG, Robson PM, Karakatsanis N, Mani V, et al. Hybrid magnetic resonance imaging and positron emission tomography with fluorodeoxyglucose to diagnose active cardiac sarcoidosis. JACC Cardiovasc Imaging. 2018;11:94–107. 10.1016/j.jcmg.2017.02.021. [PubMed: 28624396]
151. Cherry SR, Sorenson JA, Phelps ME. Physics in nuclear medecine. Philadelphia: Elsevier Science; 2003.
152. Chen BC, Legant WR, Wang K, Shao L, Milkie DE, Davidson MW, et al. Lattice light-sheet microscopy: Imaging molecules to embryos at high spatiotemporal resolution. Science. 2014 10.1126/science.1257998.
153. Ephrat P, Albert GC, Roumeliotis MB, Belton M, Prato FS, Carson JJL. Localization of spherical lesions in tumor-mimicking phantoms by 3D sparse array photoacoustic imaging. Med Phys. 2010;37:1619–28. 10.1118/1.3352785. [PubMed: 20443483]
154. James ML, Gambhir SS. A molecular imaging primer: Modalities, imaging agents, and applications. Physiol Rev. 2012;92:897–965. 10.1152/physrev.00049.2010. [PubMed: 22535898]

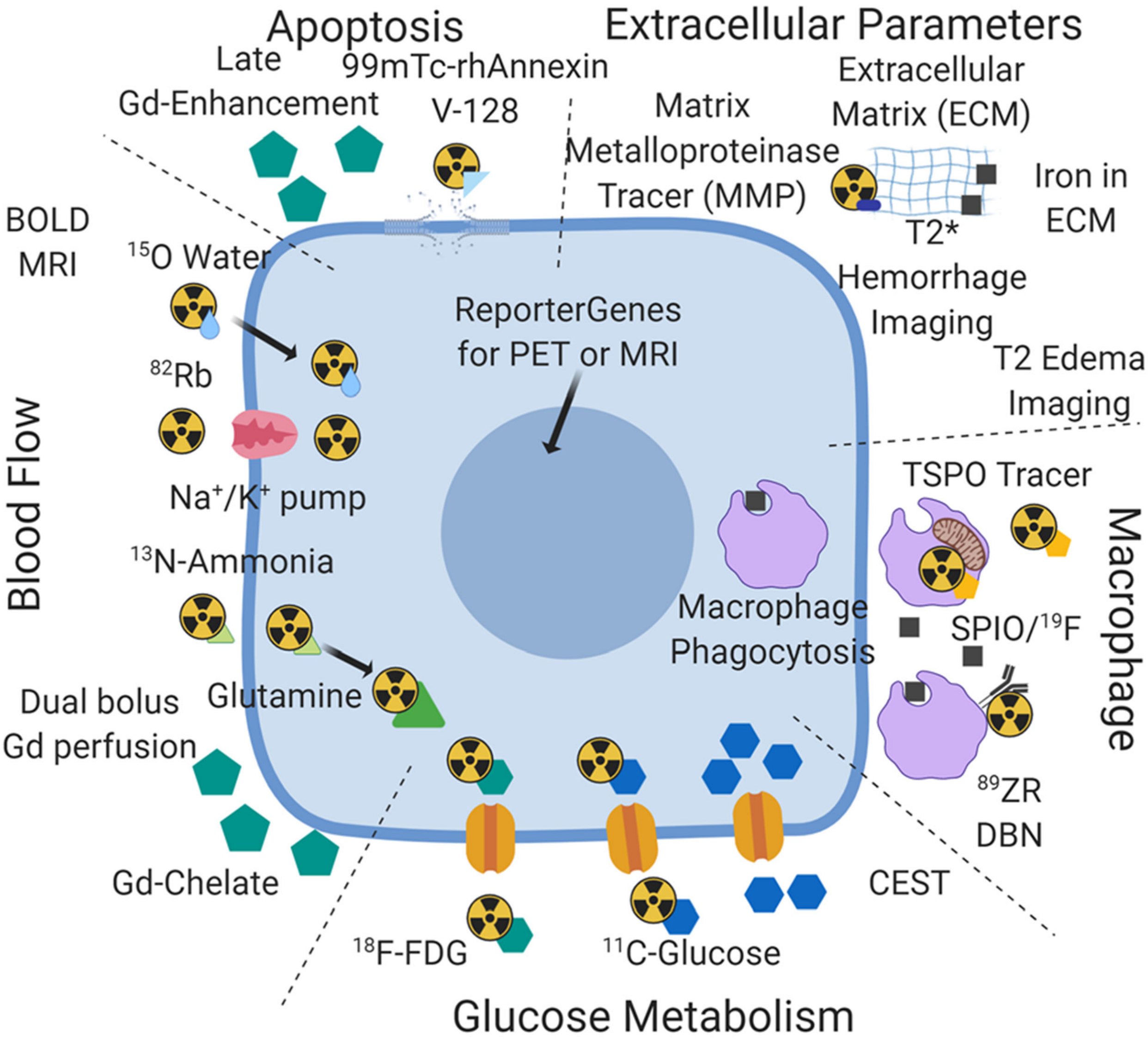

Figure 1.

Availability of PET tracers and MRI approaches for a convergent hybrid PET/MRI approach to the study of cardiac inflammation post-MI. This figure is an attempt to integrate the PET tracers and MRI approaches available for the study of inflammation post-MI under the categories of myocyte glucose metabolism, detection of inflammatory cells, measurement of blood flow, examination of changes in the extracellular matrix (not discussed in the review), and cell death (apoptosis section). The intent is to suggest a synthesis of the available independent toolbox for PET and MRI into hybrid PET/MRI.

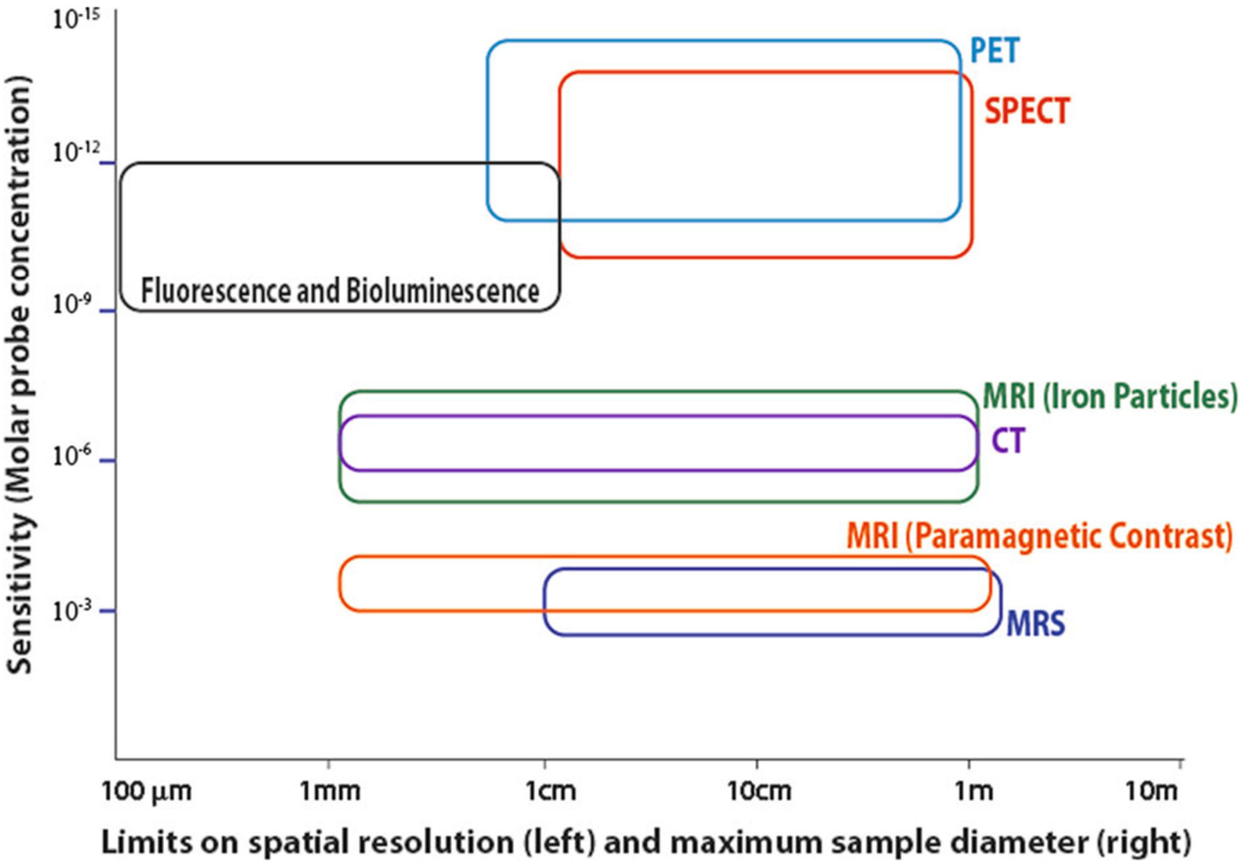

Figure 2.

Comparison of the capability of different large animal and human molecular imaging modalities. This figure uses a log-log scale of sensitivity on the vertical axis and spatial resolution on the horizontal axis to demonstrate the capabilities of several imaging modalities. The limit on spatial resolution is shown as the left edge of each shape, while the approximate maximum sample size, which is dependent on both instrument design and signal attenuation, is shown as the right edge. The height of each shape shows the range of sensitivity estimates. This figure was first published by Goldhawk et al, using data from several sources and is used with permission.[87,135–137,151–154].

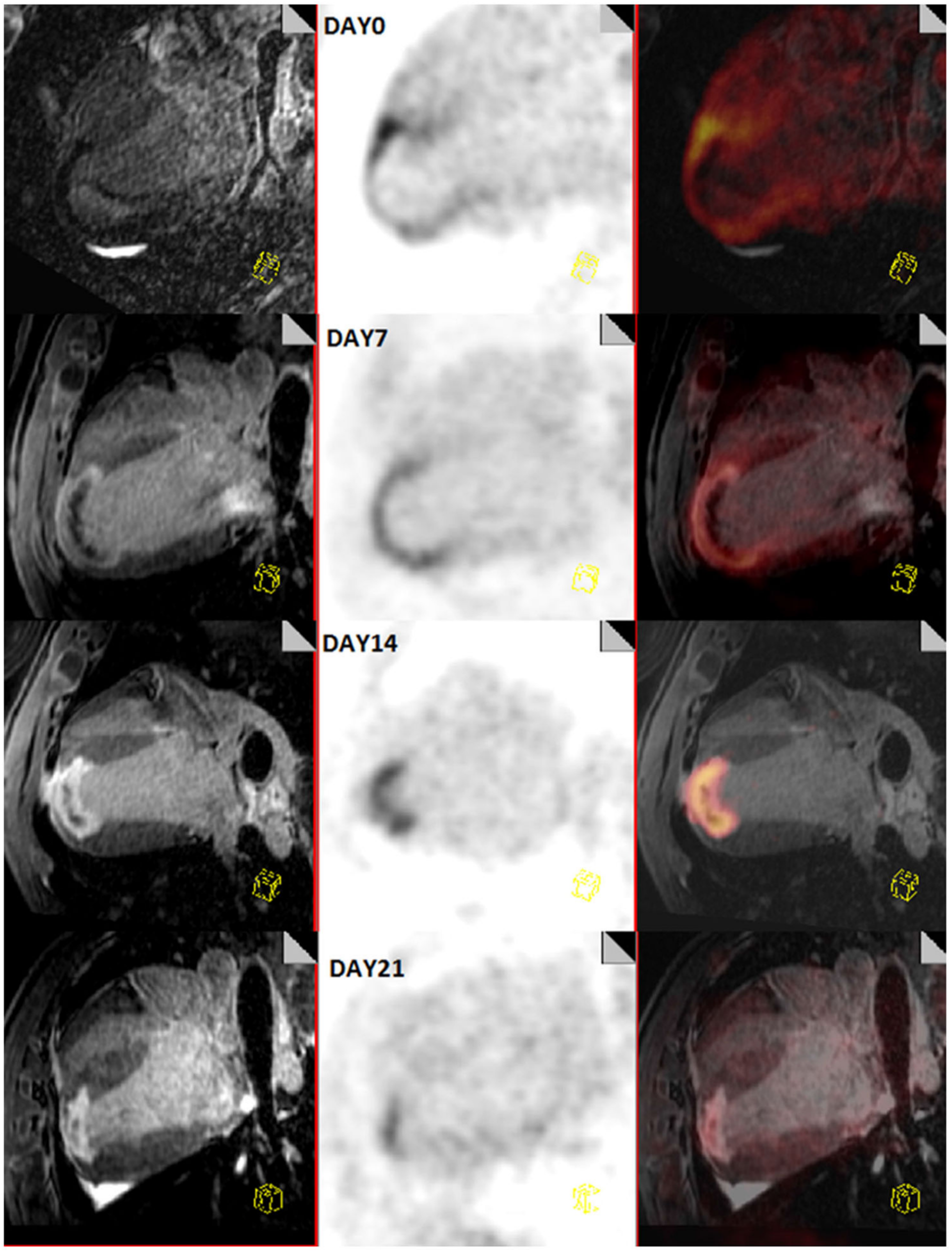

Figure 3.

Longitudinal comparison of inflammation post-MI with PET/MR in a canine model. This figure shows the progression of a myocardial infarction from day 0 (top) to day 21 (bottom). On the left are a multiplanar reconstruction of 3D T1-weighted images showing a 4-chamber view of the heart, acquired 20 minutes after a bolus injection of Gd-DTPA, in the middle is an ^{18}F-FDG image and on the right is a combined PET/MR image. Myocardial glucose uptake is suppressed by lipid infusion and heparin injection. These images show that the areas of inflammation decrease over time.

Figure 4.

Post-mortem images of the left ventricle in a canine model. Hybrid PET/MRI after constant simultaneous infusion of FDG and Gd-DTPA in a large animal model of inflammation post-MI. Registration is “Perfect” as the PET/MRI were acquired post-euthanasia. Arrows indicate center of infarct (blue) and edges of infarct (orange). Notice that inflammation by PET extends beyond the infarct into the “remote” left ventricular myocardium but is not transmural in this “remote” region. Uptake of FDG in the “remote” myocardial tissue PET images could be further improved by MRI-guided partial volume correction. Suppression was achieved through lipid infusion, heparin injection, and fasting.

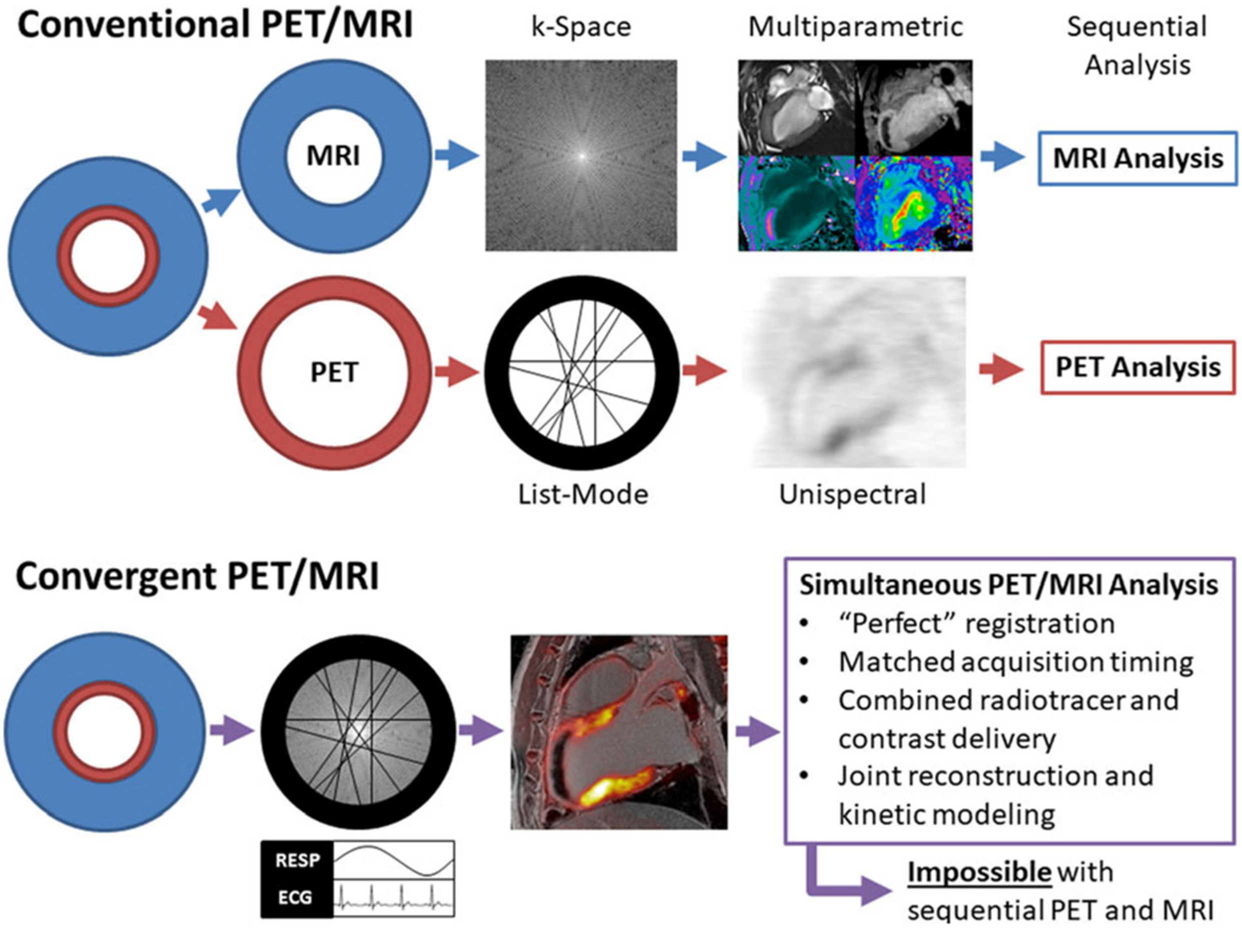

Figure 5.

Conventional vs convergent approaches to cardiac hybrid PET/MRI protocols. To date, most clinical applications of hybrid PET/MRI in cardiology have adopted protocols that were developed for sequential PET/MRI, which results in good PET and MRI images that are analyzed separately. However, good registration of PET and MRI is not always achieved. With an approach which treats hybrid PET/MRI as a new imaging modality, achieved through the convergence of the two modalities, cardiac PET/MR images could be achieved which are not possible with sequential acquisitions. An example of this potential is shown in Figure 4.

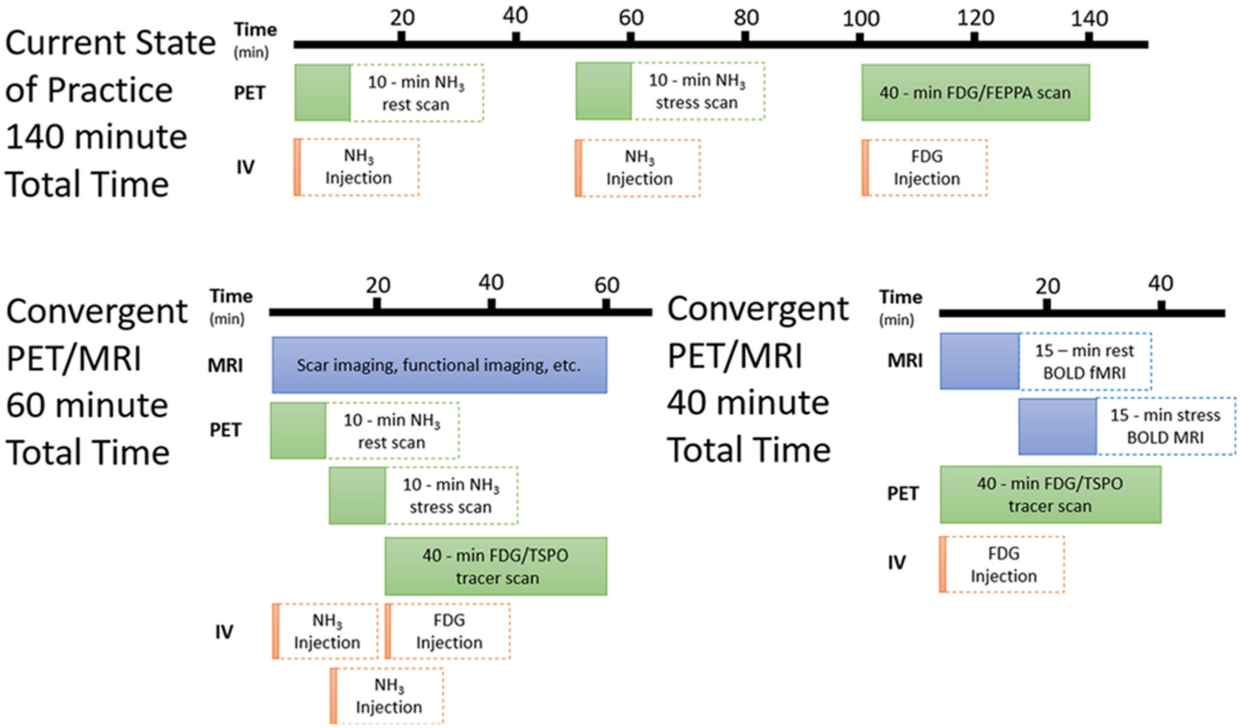

Figure 6.

Imaging myocardial perfusion reserve and inflammation with a convergent PET/MRI protocol. Using the current state of practice, imaging myocardial perfusion and inflammation sequentially would take approximately 140 minutes, unacceptably prolonging the exam. Using convergent technology, this could be reduced to 60 minutes with near-perfect registration, using a rapid dual-injection for ^{13}N-ammonia for measuring rest and stress blood flow, as suggested by Rust et al.[94] However, when injecting the tracer beforehand or using alternate tracer delivery, and using BOLD MRI instead of PET[61], it could be reduced even further, to 30 minutes or less.